



Effect of the disruption chamber geometry on the physicochemical and structural properties of water-soluble myofibrillar proteins prepared by high pressure homogenization (HPH)



Yufeng Li, Xing Chen, Siwen Xue, Ming Li, Xinglian Xu*, Minyi Han, Guanghong Zhou

Key Laboratory of Animal Products Processing, Ministry of Agriculture, Key Laboratory of Meat Processing and Quality Control, Ministry of Education, Jiangsu Synergetic Innovation Center of Meat Production and Processing, College of Food Science and Technology, Nanjing Agricultural University, Nanjing, Jiangsu, 210095, PR China

ARTICLE INFO

Keywords:

Non-thermal processing
Myofibrillar proteins
Protein structures
Microstructure
Solubility

ABSTRACT

High pressure homogenization (HPH) can solubilize myofibrillar proteins (MPs) in water. To elucidate the effect of the HPH disruption chamber geometry on the physicochemical and structural properties of MPs in water, two types of nozzle and a counter flow interaction chamber (cf) were applied to homogenize MPs aqueous solutions at pressures of 0 MPa, 103 MPa and 172 MPa HPH for 2 passes, and the physical dispersion and conformational characteristics of MPs in water were investigated. The nozzles and counter flow chamber played a major role in the solubility of MPs in water at 103 MPa and 172 MPa HPH, respectively. Turbulence and cavitation in a narrow nozzle and counter flow action resulted in a decreased MP particle size (232 nm) in water, destroyed secondary structures and exposed hydrophobic and SH groups. The solubility (98.1%) and stability of MPs in water were increased by HPH. The results showed that the required solubility of MPs in water can be achieved by adopting proper HPH disruption chamber geometry, which provides a new method on meat processing.

1. Introduction

Meat is rich in high-quality proteins and can provide all the essential amino acids for humans. Myofibrillar proteins (MPs) are the most predominant protein in skeletal muscle. Some of these proteins are insoluble in physiological saline or low ionic strength solutions and are only soluble at high salt concentrations (Krishnamurthy et al., 1996), so these proteins are known as salt proteins. Because of the harder texture of meat and meat products, the use of meat protein is not as common as the use of milk or soy protein products (Takai, Yoshizawa, Ejima, Arakawa, & Shiraki, 2013). Meat products might be utilized in various products, such as a liquid diet for elderly people and children if MPs could be solubilized in water or low ionic strength solutions (Hayakawa, Ito, Wakamatsu, Nishimura, & Hattori, 2009; Nieuwenhuizen, Weenen, Rigby, & Hetherington, 2010; Tokifuji, Matsushima, Hachisuka, & Yoshioka, 2013).

Many studies using a variety of methods have been conducted on the solubilization of MPs in water or low ionic strength solutions (Hayakawa et al., 2009; Ito, Tatsumi, Wakamatsu, Nishimura, & Hattori, 2015; Takai et al., 2013). In recent years, our group has developed a new method to solubilize MPs in water by high-pressure homogenization (HPH). The potential of HPH treatment to solubilize

chicken breast MPs in water without degradation of individual protein polypeptides has been reported (Chen, Xu, & Zhou, 2016b). In addition, the altered myosin conformation in MPs inhibits filament formation, thus contributing to the high solubility of MPs in water (Chen et al., 2016a). However, how the solubility and stability of MPs in water are affected by different HPH treatment conditions remains unclear.

High pressure homogenization (HPH) is a nonthermal technology that can produce foods with interesting functional properties (Zamora & Guamis, 2015). An HPH complex system includes a high-pressure generator, together with a pressure intensifier compressed up to 300 MPa. The homogenization chamber has different geometries, including a simple orifice plate, colliding jets or radial diffuser assemblies. In recent years, many studies have shown that different HPH disruption chamber geometries impose various effects on the structure and physicochemical properties of protein material. A correct design of the homogenization chamber may help in obtaining uniform fluid-dynamic conditions of oil/water nanoemulsions (Donsi, Sessa, & Ferrari, 2012). Subsequently, the same researchers found that the kinetics of microbial inactivation by HPH depends on the geometry of the disruption chamber (Donsi, Annunziata, & Ferrari, 2013). Some researchers investigated that the combination of pressure level and homogenising cell (HC) configurations can be used to obtain gels with

* Corresponding author.

E-mail address: xlxus@njau.edu.cn (X. Xu).

<https://doi.org/10.1016/j.lwt.2019.02.036>

Received 27 July 2018; Received in revised form 11 February 2019; Accepted 11 February 2019

Available online 12 February 2019

0023-6438/ © 2019 Elsevier Ltd. All rights reserved.

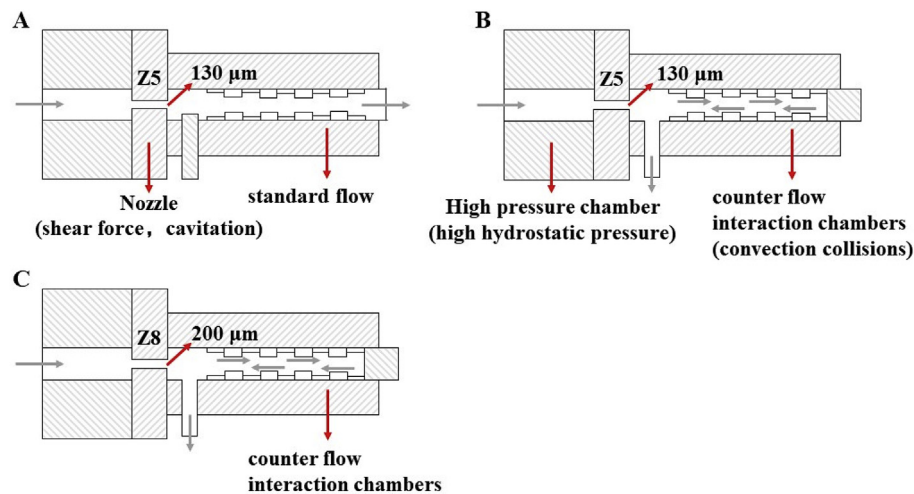


Fig. 1. Simplified sketch of the different geometries of the homogenization chambers tested (Donsi et al., 2012). Note: A: Z5 configuration (130 μm nozzle, standard flow); B: Z5-cf configuration (130 μm nozzle, counter flow); C: Z8 configuration (200 μm nozzle, standard flow).

specific rheological properties (Alvarez-Sabatel, Mara \tilde{n} on, & Arboleya, 2015). In addition to HPH interaction chambers, HPH pressure also plays a role on the structural and functional properties of protein materials (Saricaoglu, Gul, Tural, & Turhan, 2017). The physicochemical stability of egg/dairy emulsion is directly related to the HPH pressure applied during the process (Marco-Mol \acute{e} s, Hernando, Llorca, & P \acute{e} rez-Munuera, 2012). These results showed that both the selection of the HPH interaction chamber and the regulation of HPH pressures are critical for the resultant structural and functional properties of food materials.

Although our group previously showed that 103 MPa for 2 passes HPH is an efficient technique for the solubilization of MPs in water (Chen et al., 2016b), but the level of solubility and how it responds to the type of disruption chamber geometry and HPH pressure remains unclear. We think that the effect of the various disruption chamber geometries on the physicochemical and structural properties of MPs in water is worth investigation. Liquid materials are subjected to 2 or 3 types of physical effects during HPH. The disruption chamber is shown in Fig. 1, and it includes a high-pressure chamber, nozzle and counter flow (cf) interaction chamber. Different disruption chambers might have various effects on the physical properties of the materials. The high-pressure chamber provides high hydrostatic pressure, the nozzle generates a strong shear force and cavitation, and the counter flow interaction chamber produces convection collisions. In addition, the disruption sequence of HPH on the liquid material changes with different disruption chamber geometries. We speculated that different HPH disruption chamber geometries might result in various effects on MPs in water. Therefore, the objective of the present work was to study the effect of 103 MPa and 172 MPa HPH pressures for two passes on MP suspensions, three different disruption chamber geometries (Z5, Z5-cf, Z8-cf) was applied. The effects of HPH disruption chamber geometry on the solubility and stability of MPs in water were investigated in this study, it will be helpful for the selection and design of interaction chambers for tailor-made aqueous MP suspensions for further utilization.

2. Materials and methods

2.1. Materials

The chicken breasts were purchased 36 h postmortem from local market (Sushi Food Co., Ltd., Nanjing, China), and were stored under $-20\text{ }^{\circ}\text{C}$ till required (within one week). Bovine serum albumin (BSA), β -mercaptoethanol (β -ME), 8-Anilino-1-naphthalenesulfonic acid

(ANS), 5,5'-Dithiobis-(2-nitrobenzoic acid) (DTNB) and phosphotungstic acid was provided by Sigma (Sigma Aldrich, St. Louis, MO, USA). Protein maker and 4–12 g/mL gel of SDS-PAGE was provided by Genscript (Genscript Co., Ltd., Nanjing, China).

2.2. Preparation of chicken breast myofibrils

The frozen chicken breast was thawed for approximately 12 h at $4\text{ }^{\circ}\text{C}$. After removing the connective and adipose tissues, the chicken breast was ground three times in a chilled cutter (Grindomix GM 200, Retsch, Haan, Germany) for 10 s each time at a speed of 3000 rpm. The minced meat (100 g) was washed four times with three buffer solutions. The sediment of each step was recovered by centrifugation at 10,000 g for 10 min at $4\text{ }^{\circ}\text{C}$. In the first, the minced meat was mixed with 1 L 25 mmol/L NaCl buffer solution (5 mmol/L EDTANa $_2$, 5 mmol/L Tris-HCl, pH 7.5) and processed for 3 min in a tissue crusher. In the second step, after mixing with 500 mL 0.1 M NaCl buffer solution and 2.5 mL TritonX-100, the suspension was homogenized (Ultraturrax T25, IKA, Staufen, Germany) of 1 min. In the third step, the sediment was mixed with 500 mL 0.1 mol/L NaCl buffer solution and homogenized for 30 s (Ultraturrax T25, IKA, Staufen, Germany). Before centrifugation, the suspension was filtered through 3 layers of gauze to remove the connective tissue and lipids. In the final step, the sediment was mixed with 1 L 2.5 mmol/L NaCl buffer solution and homogenized for 30 s (Ultraturrax T25, IKA, Staufen, Germany). After the final step, the collected sediment was deemed the myofibril fraction.

2.3. Preparation of MP dispersion in water by HPH

The MP was mixed with cold ($4\text{ }^{\circ}\text{C}$) deionized, distilled water, homogenized (Ultraturrax T25, IKA, Staufen, Germany) at 8000 rpm for 2 min. The concentration of MP suspension was adjusted to 5 mg/mL.

HPH was implemented using a high pressure homogenizer (Mini DeBee, Bee International, South Easton, MA, USA) equipped with a single-pressure intensifier and 3 homogenization chamber configurations (Genizer, Irvine, CA, USA). The geometry and schematic of this homogenising cell are described in Fig. 1, both the Z5 (Fig. 1A) and Z5-cf (Fig. 1B) configuration has a 130 μm nozzle, but the interaction chamber of these configurations is different (standard flow, counter flow). The Z8-cf (Fig. 1C) configuration consists in 200 μm nozzle and counter flow interaction chamber. The MP suspension was passed through the homogenization chamber at a constant pressure, 103 MPa and 172 MPa, for 2 passes. The inlet temperature of samples was $4\text{ }^{\circ}\text{C}$. A heat exchanger with a rapid cooling system was implemented in the

homogenizer. The final samples were rapidly stored at 4 °C for further analysis. The untreated MP suspension was used as the control.

2.4. Solubility

The MP suspension was centrifuged at 20,000 g for 20 min at 4 °C (Beckman Coulter model Avanti J-26SXP, Beckman Instruments Inc., Atlanta, GA, USA). Protein solubility was then calculated as percentage of protein content in the supernatant relative to total protein content in the sample. To test the stability of the MP suspension, it was stored at 4 °C for 9 days.

2.5. SDS-polyacrylamide gel electrophoresis

The protein profiles of samples were determined by SDS-polyacrylamide gel electrophoresis (SDS-PAGE). SDS-PAGE was run with a precast 4–12 g/mL gel. Protein samples (2 mg/mL) were mixed with an equal volume of sample buffer with 55.7 g/L β -ME and boiled for 4 min. Each well was loaded with 10 μ L of sample or marker. Electrophoretic analysis was performed (Mini-PROTEAN II, Bio-Rad Laboratories Inc., Hercules, CA, USA) at a constant voltage of 120 V for 1 h. The stained gel was scanned using an Imager Scanner III (EU-88, Epson, Nagano-ken, Japan), and the densities of bands were calculated using the software 'Quantity One Analysis' (Bio-Rad, Laboratories Inc., Hercules, CA, USA).

2.6. Dynamic light scattering (DLS) measurement of particle size

DLS measurement was performed as previously reported (Chen et al., 2016b) with a slight modification. MP suspension particle size was determined using Zetasizer (Nano ZS90, Malvern Instruments, Royston, UK). The concentration of MP samples was adjusted to 0.5 mg/mL, placed in a 1-cm path-length quartz cuvette and subjected to DLS measurement with a detection angle of 90° at 25 \pm 0.1 °C and obtain the mean particle size.

2.7. Rheological measurements

The rheological measurements of MP suspensions were performed using a rheometer (Physica MCR301, Anton Paar Corporation, Graz, Austria) fitted with parallel plate geometry of 50 mm diameter (Zhao et al., 2014). The measurements were carried out using a gap distance of 0.5 mm. The samples were equilibrated in parallel plates for 30 s prior to measurements to obtain a desirable temperature of 25 °C. Viscosity was then recorded as the shear rate that linearly increased from 1 s⁻¹ to 1000 s⁻¹ (Liu, Wang, & Zhang, 2015).

2.8. Atomic force microscopy (AFM) imaging and analysis

AFM images were obtained according to a previous report (Zhong et al., 2015) using a Peak Force Tapping technology AFM (Dimension Icon, Bruker Corporation, Karlsruhe, Germany) equipped with a Si₃N₄ cantilevered scanner under atmospheric pressure at room temperature (25 °C). The linear scanning rate was optimized at 1 Hz with a scan resolution of 512 samples per line. The samples were continuously diluted to 0.05 mg/mL with ultrapure deionized water, and 5 μ L MP aqueous solution was cast on freshly cleaved mica and allowed to dry in ambient air for 20 min, then subjected to AFM analysis. All height images were treated with the "flatten" function using Nanoscope Analysis software (Version 1.40, Bruker Corporation, Karlsruhe, Germany) prior to analysis.

2.9. Transmission electron microscopy (TEM)

All the MP suspensions were diluted to 10 μ g/mL. The samples were dropped onto wax plates and covered with copper wire meshes plated

with carbon films. The drops were in contact with the carbon films. After using a filter paper wick for 30 s to the edge of the copper wire mesh to absorb extra liquid, the samples were negatively stained with 30 g/L phosphotungstic acid aqueous solution for 1 min when slightly dry, the extra solution was removed with a piece of filter paper. The copper wire meshes (the specimens) were illuminated under a filament lamp for 10 min to dry, and then, the samples were carried out using a TEM (Tecnai 12, Philips company, Eindhoven, Netherlands) at an accelerating voltage of 120 kV (Sharp & Offer, 1992).

2.10. Secondary structure analysis by circular dichroism (CD)

The CD spectrum was measured using a spectropolarimeter (Jasco J-715, Jasco Co. Ltd., Tokyo, Japan). Soluble MPs (0.3 mg/mL) were transferred to a quartz cell with a 0.1 cm light-path. Molecular ellipticity was measured in the range from 200 to 240 nm at a scan rate of 20 nm/min at a regulated temperature. The percentages of α -helix structures were determined using the protein secondary structure estimation program provided with the Jasco J-715 spectro-polarimeter.

2.11. Reactive sulfhydryl (SH) groups and surface hydrophobicity determination

The method determined according to previously described procedures (Chen et al., 2016a). DTNB solution (50 μ L in 20 mmol/L phosphate buffer, pH 8.0) was added to 4 mL samples (1 mg/mL) and incubated for 20 min at 25 °C. The absorbance of the mixture was measured at 412 nm with a Microplate Reader (SpectraMax M2, Molecular Devices Limited, San Jose, CA, USA). The sulfhydryl contents were obtained by dividing the absorbance by the molar extinction coefficient (EM = 13,600) and expressed as micromoles of SH per 100 mg protein.

The surface hydrophobicity of MPs in water was determined as previously described (Chen et al., 2014) with slight modifications. The surface hydrophobicity was tested using ANS. A total of 10 μ L of 15 mmol/L ANS solution (in 0.1 mol/L phosphate buffer, pH 7.0) was added to 2 mL of each sample (1 mg/mL). After incubating for 20 min in the dark, fluorescence was determined (SpectraMax M2, Molecular Devices Limited, San Jose, CA, USA) using an excitation wavelength of 380 nm and an emission wavelength in the range of 410–570 nm at a 5 nm/s scanning speed. The surface hydrophobicity was expressed as fluorescence intensity (arbitrary units, a.u.)

2.12. Data analysis

The data were analyzed with the Statistical Analysis System (SAS Institute Inc., Cary, NC, USA). A variance test (ANOVA) was performed with a significance level of $P < 0.05$. Duncan's multiple range test was used to evaluate the differences between treatments.

3. Results and discussion

3.1. Protein solubility

The effect of different HPH disruption chamber geometries on the solubility of MPs in water is shown in Table 1. The solubility of MPs was rather low (20.0%) when the MP suspension was not treated with HPH, and the solubility of HPH-treated samples was obviously higher following HPH, which was consistent with our previous results (Chen et al., 2016b; Saricaoglu et al., 2017). There was no significant difference between Z5 and Z5-cf when the pressure was 103 MPa, but the solubility of Z8-cf was obviously lower than the others. This result indicated that the bore diameter of the nozzle might play a more important role at 103 MPa HPH treatment. We postulate that the effect of the counter flow interaction chamber was not obvious at 103 MPa. The solubility of MPs in water was significantly higher when the pressure

Table 1

Solubility of myofibrillar protein (MPs) in water after 103 MPa and 172 MPa high pressure homogenization (HPH) treatment with different disruption chambers.

Pressure (MPa)	Solubility (%)		
	Z5	Z5-cf	Z8-cf
0	18.80 ± 0.97 ^e	18.80 ± 0.97 ^e	18.80 ± 0.97 ^e
103	87.37 ± 0.73 ^c	87.30 ± 2.33 ^c	80.11 ± 3.10 ^d
172	93.63 ± 2.24 ^b	98.10 ± 0.44 ^a	97.36 ± 1.56 ^a

Note: Values were mean of triplicate values ± S.D. Different letter in row indicate statistical differences ($P < 0.05$).

Control: non-HPH treated sample; Z5: 130 µm nozzle and standard flow; Z5-cf: 130 µm nozzle and counter flow; Z8-cf: 200 µm nozzle and counter flow.

Table 2

Stability of myofibrillar protein (MPs) in water after 103 MPa high pressure homogenization (HPH) treatment with different disruption chambers.

Storage time (day)	Control	Solubility (%)		
		Z5	Z5-cf	Z8-cf
0	18.80 ± 0.97 ⁱ	87.37 ± 0.73 ^a	87.31 ± 2.33 ^a	80.11 ± 3.10 ^b
3	18.45 ± 0.40 ⁱ	81.44 ± 0.59 ^b	71.49 ± 0.57 ^c	65.68 ± 0.85 ^d
6	17.06 ± 0.84 ⁱ	58.39 ± 1.14 ^f	62.81 ± 1.20 ^c	49.48 ± 0.87 ^h
9	16.83 ± 0.33 ⁱ	52.50 ± 1.50 ^g	54.86 ± 0.91 ^g	49.15 ± 0.50 ^h

Note: Values were mean of triplicate values ± S.D. Different letter in row indicate statistical differences ($P < 0.05$).

Control: non-HPH treated sample; Z5: 130 µm nozzle and standard flow; Z5-cf: 130 µm nozzle and counter flow; Z8-cf: 200 µm nozzle and counter flow.

was raised to 172 MPa. This finding indicated that 172 MPa HPH effectively increased the solubility of MPs in water. Interestingly, the solubility of Z5 was the lowest among the three types of chambers, and there was no significant difference between Z5-cf and Z8-cf. This result showed that the counter flow interaction chamber is the main factor influencing the solubility of MPs in water during 172 MPa HPH. These data indicate that the nozzle and counter flow interaction chamber might play more important roles in the solubility of MPs in water with 103 MPa and 172 MPa HPH treatment.

The stability of MPs in water is shown in Tables 2–3. All the HPH-treated samples showed a significant decrease in solubility after storage, this phenomenon has also been reported in previous research (Chen et al., 2016b). At 103 MPa HPH, the Z8-cf sample was the least stable among all HPH-treated samples. This trend was the same as the differences in MP solubility. Compared with the 103 MPa HPH treatment, all the HPH-treated samples showed relatively good stability during storage when the pressure was 172 MPa. As previously mentioned, the HPH at 207 MPa induced the appearance of turbulence, cavitation and high shear forces (Donsi et al., 2012) that might break the inulin nuclei (Ronkart et al., 2010). The 100 g/L HPH-treated samples (103 and 207 MPa) with the standard flow configuration exhibited a homogeneous white structure along the entire sample (Alvarez-Sabatel et al., 2015). Meanwhile, most of the proteins (more than 80.0%) remained in the water after 9 days. Compared to the Z5 and Z8-cf, the solubility of Z5-cf was much lower with storage, and the final solubility of Z5-cf was also the lowest, which contrasted with the

Table 3

Stability of myofibrillar protein (MPs) in water after 172 MPa high pressure homogenization (HPH) treatment with different disruption chambers.

Storage time (day)	Solubility (%)		
	Control	Z5	Z8-cf
0	18.80 ± 0.97 ^f	98.10 ± 0.44 ^a	97.36 ± 1.56 ^{ab}
3	18.45 ± 0.40 ^f	97.64 ± 2.94 ^{ab}	95.23 ± 1.68 ^{abc}
6	17.06 ± 0.84 ^f	96.32 ± 1.05 ^{abc}	96.96 ± 3.25 ^{ab}
9	16.83 ± 0.33 ^f	93.63 ± 2.24 ^c	95.11 ± 1.50 ^{bc}

Note: Values were mean of triplicate values ± S.D. Different letter in row indicate statistical differences ($P < 0.05$).

Control: non-HPH treated sample; Z5: 130 µm nozzle and standard flow; Z5-cf: 130 µm nozzle and counter flow; Z8-cf: 200 µm nozzle and counter flow.

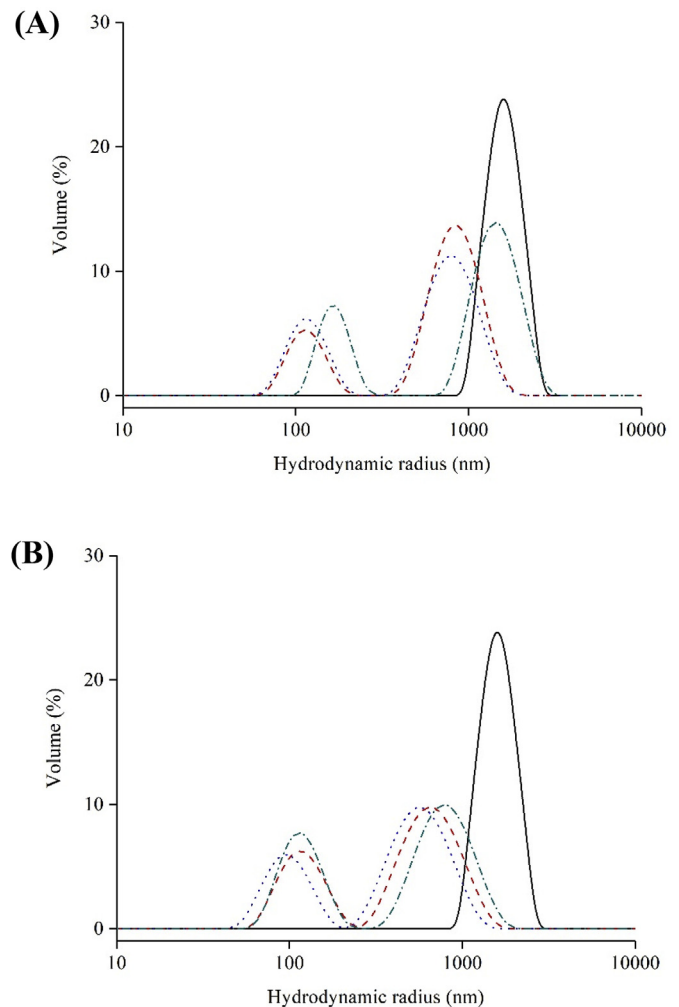


Fig. 2. Particle size distribution of MPs in water treated by high pressure homogenization (HPH) at 103 MPa (A) and 172 MPa (B). Note: Control (continuous line); Z5 configuration (dashed line); Z5-cf configuration (dot line); Z8-cf configuration (dot-dashed line).

Table 4

Z-average of myofibrillar protein (MPs) in water after 103 MPa and 172 MPa high pressure homogenization (HPH) treatment with disruption chambers.

Pressure (MPa)	Z-average (nm)*		
	Z5	Z5-cf	Z8-cf
0	1616 ± 294 ^a	1616 ± 294 ^a	1616 ± 294 ^a
103	412 ± 10 ^{bc}	371 ± 33 ^c	430 ± 45 ^b
172	249 ± 6 ^d	247 ± 39 ^d	232 ± 16 ^d

Note: Values were mean of triplicate values ± S.D. Different letter in row indicate statistical differences ($P < 0.05$).

Control: non-HPH treated sample; Z5: 130 µm nozzle and standard flow; Z5-cf: 130 µm nozzle and counter flow; Z8-cf: 200 µm nozzle and counter flow.* Z-average hydrodynamic diameter obtained by DLS.

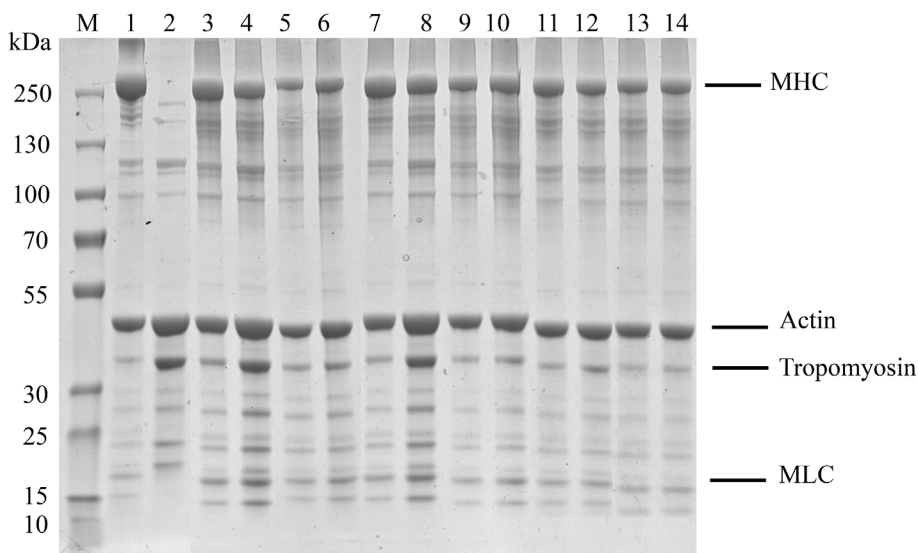


Fig. 3. SDS-PAGE pattern of myofibrillar proteins (MPs) in water treated by different high pressure homogenization (HPH) disruption chambers and pressures. Note: Lane M: molecular weight marker; Lane 1: Control (non-HPH treated sample); Lane 2: supernatant of control after centrifugation (20,000 g for 20 min at 4 °C); Lane 3: 103 MPa HPH treated suspension (Z5); Lane 4: supernatant of 103 MPa HPH treated suspension after centrifugation (Z5); Lane 5: 172 MPa HPH treated suspension (Z5); Lane 6: supernatant of 172 MPa HPH treated suspension after centrifugation (Z5); Lane 7: 103 MPa HPH treated suspension (Z5-cf); Lane 8: supernatant of 103 MPa HPH treated suspension after centrifugation (Z5-cf); Lane 9: 172 MPa HPH treated suspension (Z5-cf); Lane 10: supernatant of 172 MPa HPH treated suspension after centrifugation (Z5-cf); Lane 11: 103 MPa HPH treated suspension (Z8-cf); Lane 12: supernatant of 103 MPa HPH treated suspension after centrifugation (Z8-cf); Lane 13: 172 MPa HPH treated suspension (Z8-cf); Lane 14: supernatant of 172 MPa HPH treated suspension after centrifugation (Z8-cf). MHC: myosin heavy chain, MLC: myosin light chain.

solubility at the 0 day. The standard flow chamber (Z5) exhibited a slightly better performance than the other geometries for all the tested emulsifiers when the pressure was below 280 MPa (Alvarez-Sabatel et al., 2015). Therefore, it's probably due to effect of the “over processing” (Saricaoglu et al., 2017), which was caused by the narrow nozzle and counter flow (Z5-cf). Overall, the response regularity of the disruption chamber geometry on stability of MPs in water was different from the solubility effect, and it is possible to adjust the solubility and stability of MPs in water by choosing a suitable disruption chamber.

3.2. Particle size distribution (PSD)

The PSD and Z-average of MPs in water are given in Fig. 2 and Table 4. The non-HPH treated sample had a large Z-average (1616 nm) and showed highly ordered myofibril structures with various large particle sizes in water. Compared with the control, the Z-average of HPH-treated samples showed a smaller particle size (Table 4). This finding indicated that HPH reduced the particle size of MPs in water. The PSD showed a slow shift toward left of the control after HPH treatment with various disruption chamber geometries, and all HPH-treated samples showed a wide distribution of large particle sizes. The distribution of the control was unimodal, with protein aggregates higher than 1000 nm. The bimodal PSD of MPs in water might be caused by the release of monomer species (myosin or actin) and myofibrils (thick filaments; Chen et al., 2016b). The mechanical forces imparted by HPH disrupt the structure of proteins and macromolecules and cause the reduction of protein particle size (Dumay et al., 2013; Song, Zhou, Fu, Chen, & Wu, 2013). In the case of the 103 MPa HPH-treated sample, the performance of Z5-cf was the best (371 nm; Table 4), and the Z-average of Z8-cf was the largest. This finding showed that the wide bore diameter (200 μm) nozzle and counter flow chamber had less effect in reducing the particle size of MPs in water. The reason for this result is probably related to the pressure, which might not have been high enough to produce counter flow interactions, and the nozzle played a major role in HPH. Compared to previous reports, our results showed that the particle size of MPs in water further decreased when the pressure was increased to 172 MPa, the Z-average significantly decreased to approximately 240 nm and there was no difference among the three disruption chamber geometries. These data indicated that the different disruption chamber geometries could have different effects on the particle size of MPs in water and improve homogeneity after HPH.

3.3. Protein profile

The SDS-PAGE patterns of MPs in water are shown in Fig. 3. The typical polypeptide composition of MPs in the control can be seen in lane 1 (Fig. 3). The protein bands corresponding to marker were evident in the control and HPH-treated samples. The supernatant of control obtained by centrifugation showed quite a low concentration of protein (Lane 2 in Fig. 3). However, in the HPH-treated samples, most of the proteins remained in the supernatant (Lanes 4, 6, 8, 10, 12 and 14 in Fig. 3), and there was no difference in polypeptide composition between the control and HPH-treated samples. The results showed that HPH treatment with different disruption chamber geometries solubilized MPs in water without individual protein degradation.

3.4. Rheological property

The flow behavior of MPs in water is shown in Fig. 4. The viscosity of the control was much higher than HPH-treated samples at all shear rates. The results presented in Fig. 4A suggested that the 103 MPa HPH-treated samples had shear-thinning or pseudo-plastic behavior. The pseudo-plastic behavior was previously reported for myofibrillar proteins (Chapleau & de Lamballerie-Anton, 2003; Chen et al., 2016b; Saricaoglu et al., 2017). When the pressure was 172 MPa (Fig. 4B), the viscosity of all HPH-treated samples was much lower and presented Newtonian fluid properties in the shear rate range. These observations could be attributed to the decrease of the particle size of MPs in water and the high solubility of MPs in water induced by HPH. However, it is interesting that the viscosity of the Z5-cf sample was the lowest in 103 MPa and 172 MPa HPH treatment, which suggests that the narrow bore diameter of the nozzle and counter flow action could accelerate the protein-protein interactions in MP suspensions, thus increasing the flow and dispersibility of MPs in water. It has been reported that strong physical forces including shear, turbulence, impact and cavitation are imposed on the liquid medium by HPH, modifying the flow behaviors of MP suspensions (Song, Zhou, Wu, Fu, & Chen, 2013; Sørensen et al., 2014). In conclusion, the flow rate of MPs in water was increased by high pressure (172 MPa) HPH. The narrow nozzle bore diameter resulted in MP suspensions with lower viscosity, leading to a faster flow rate and intensifying the collision effect in the counter flow chamber. The interaction of narrow nozzle could destroy the myofibril structure and protein-protein interactions, increasing the homogeneity and solubility of MPs in water.

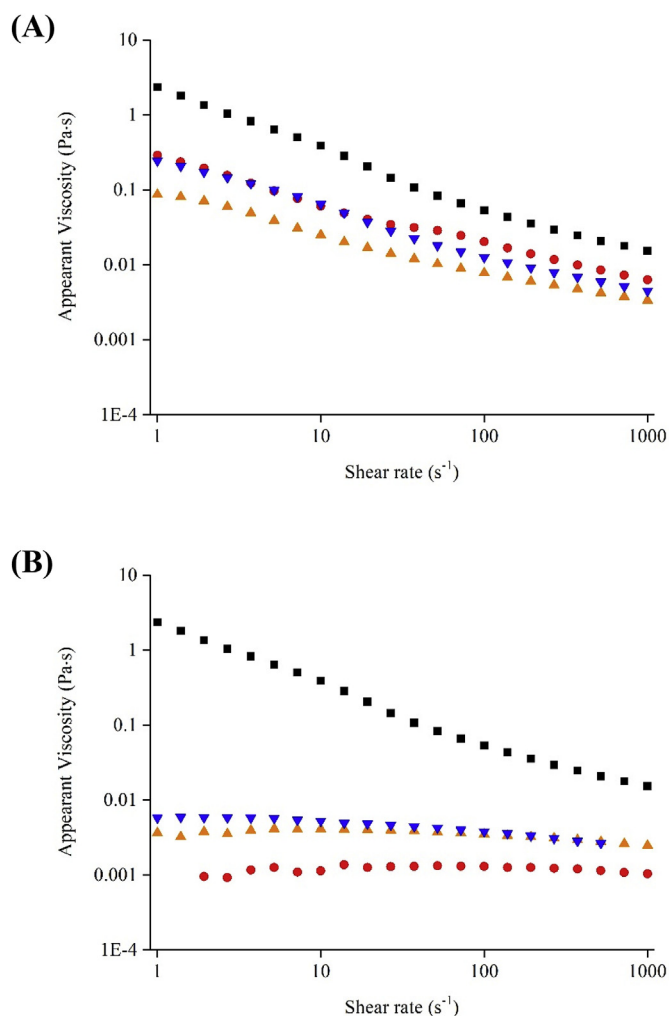


Fig. 4. Steady-state properties of myofibrillar protein (MP) suspensions (5 mg/mL) treated at 103 MPa (A) and 172 MPa (B) high pressure homogenization (HPH) treatment with different disruption chamber geometries, shear rate that linearly increased from 1 s^{-1} to 1000 s^{-1} . Note: Control (black square); Z5 configuration (red circle); Z5-cf configuration (orange triangle); Z8-cf configuration (blue triangle). (For interpretation of the references to colour in this figure legend, the reader is referred to the Web version of this article.)

3.5. Microstructure of MPs in water

AFM and TEM images are presented in Figs. 5 and 6, showing morphological differences among MP suspension microstructure after HPH with various disruption chamber geometries. At Figs. 5A and 6A, it was observed that some myofibrils with highly ordered structures remained in MP suspensions, which had a relatively homogeneous dissociated threadlike network structure (Chen et al., 2016b; Ito et al., 2015). It is obvious that the structure of myofibrils was completely disrupted to some monomer or oligomer proteins after HPH (Fig. 6), which length ranged from approximately 100–400 nm. The height of the particles in MP suspensions was 20 nm or less, which was lower than that found in our previous study (Chen et al., 2016a). Upon 103 MPa HPH treatment, myofibril protein was disrupted, showing bead-like monomers or oligomers in the HPH treated samples, and the particle height was further reduced to below 20 nm. However, there were some larger protein molecules and polymers remained in the Z8-cf suspension (Fig. 6F). The tendency of disruption of the filaments was more obvious as the pressure increased (172 MPa), at the same time, due to the interaction of the counter flow chamber, the slender filaments of Z5-cf and Z8-cf were disrupted to some monomer or oligomer proteins

(Fig. 6E and G) with lower particle height (below 5 nm) than 103 MPa HPH. The higher pressure and different disruption chamber might be a main cause of this difference. As mentioned earlier, HPH can effectively change the microstructure of myofibrils and reduce protein particle size under higher pressure and increase the dispersion of MPs in water. These results might explain the high solubility and stability of MPs in water.

3.6. Reactive sulfhydryl (SH) groups and surface hydrophobicity of MPs in water

To confirm changes in the tertiary structure and stability of MPs in water, reactive SH groups and surface hydrophobicity of MPs in water were determined (Table 5; Fig. 7). The SH groups and surface hydrophobicity of MPs in water were obviously lower after HPH treatment than were the control. The results were similar to the previous studies (Liu & Kuo, 2016; Liu et al., 2010). As shown in Table 5, The Z8-cf exhibited the fewest reactive SH groups and lowest hydrophobicity, it is indicated that the unfolding level of MPs structures in Z5 and Z5-cf was higher than Z8-cf. Turbulence and cavitation phenomena were predominant mechanisms in HPH at the outlet of the valve gap (Floury, Bellettre, Legrand, & Desrumaux, 2004). The narrow valve gap of Z5 and Z5-cf might give rise to the dissociation, aggregation and rearrangement of MPs in water, leading to the exposure of reactive SH groups and hydrophobic groups from the interior of the native protein. The reactive SH groups and surface hydrophobicity of HPH-treated samples were both significantly higher after HPH at 172 MPa. Recent studies have shown that high hydrostatic pressure leads water to permeate the interior of the protein and modify the protein conformation by affecting hydrogen and hydrophobic interactions, thus disrupting the tertiary structures of MPs (Chen et al., 2014; Zhang, Yang, Tang, Chen, & You, 2015). In this study, a higher pressure caused the unfolding of MPs and increased the number of surface SH and hydrophobic groups.

The stability of Z8-cf was lower than that of the other samples (Table 2) with the 103 MPa HPH treatment, whereas the stability of Z5-cf was the lowest among all the samples treated by 172 MPa HPH (Table 3). The basic mechanism for this remains unclear, but we observed that the changes in stability were closely related to the initial conformational changes of protein induced by HPH, especially regarding SH groups and surface hydrophobicity. At 103 MPa HPH, the Z8-cf samples generated fewer SH groups and lower surface hydrophobicity than did the Z5 and Z5-cf (Fig. 7). Similarly, the Z5-cf samples, which showed poorer stability at 172 MPa, produced fewer SH groups and lower surface hydrophobicity than did Z5 and Z8-cf (Fig. 7). The mechanical effects of the nozzle and counter flow, such as shearing, cavitation and impact, combined with the thermal action would cause protein denaturation to a certain degree, resulting in a decrease in the SH groups and surface hydrophobicity of the MPs (Fig. 7). Accumulation of denatured proteins and thereby their re-association could lead to poor stability during storage.

3.7. Secondary structures

The secondary structure of the MPs in water was determined using circular dichroism (Table 6). After 103 MPa HPH, the α -helix structure content was significantly lower, which was coupled with an increase in β -sheets, β -turns and random coils. This result confirmed a previous finding that the conformational changes under HPH promoted a loss of helicity of MPs in water (Chen et al., 2016a). There was no significant difference in the α -helix content of Z5 and Z5-cf when the pressure was 103 MPa. However, the Z8-cf suspension had the highest α -helix content (50.5%). The α -helical content of HPH-treated samples was even lower when the pressure was 172 MPa (42.4%, 41.4% and 42.0%). This result is consistent with the finding in rabbit myosin and myofibrillar protein by the HPP (Chapleau, Mangavel, Compoin, & de Lamballerie-

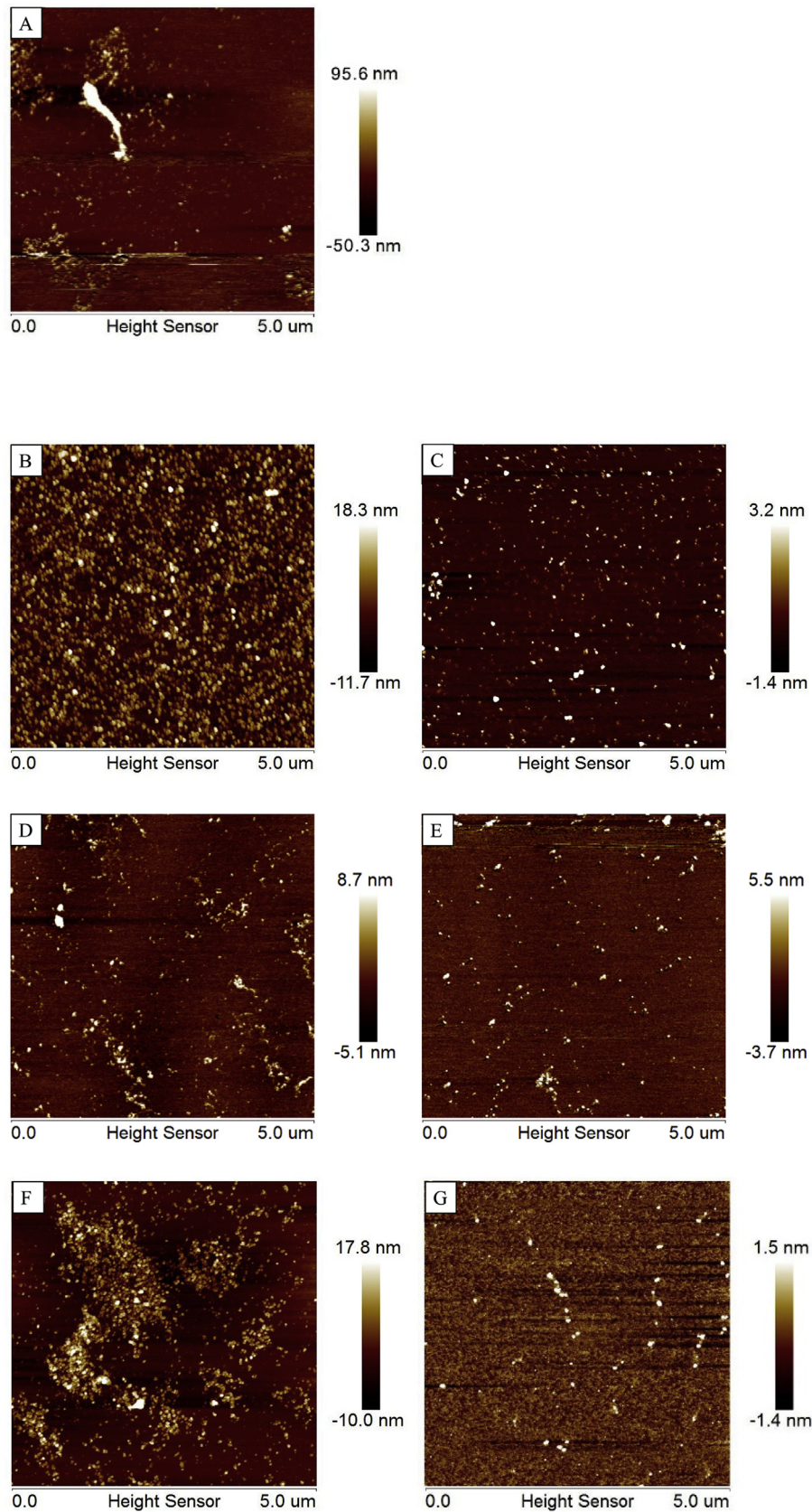


Fig. 5. The representative AFM images of myofibrillar protein (MP) suspensions treated at various high pressure homogenization (HPH) disruption chamber geometries. Note: A: Control (non-HPH treated sample); B: Z5 configuration (103 MPa); C: Z5 configuration (172 MPa); D: Z5-cf configuration (103 MPa); E: Z5-cf configuration (172 MPa); F: Z8-cf configuration (103 MPa); G: Z8-cf configuration (172 MPa).

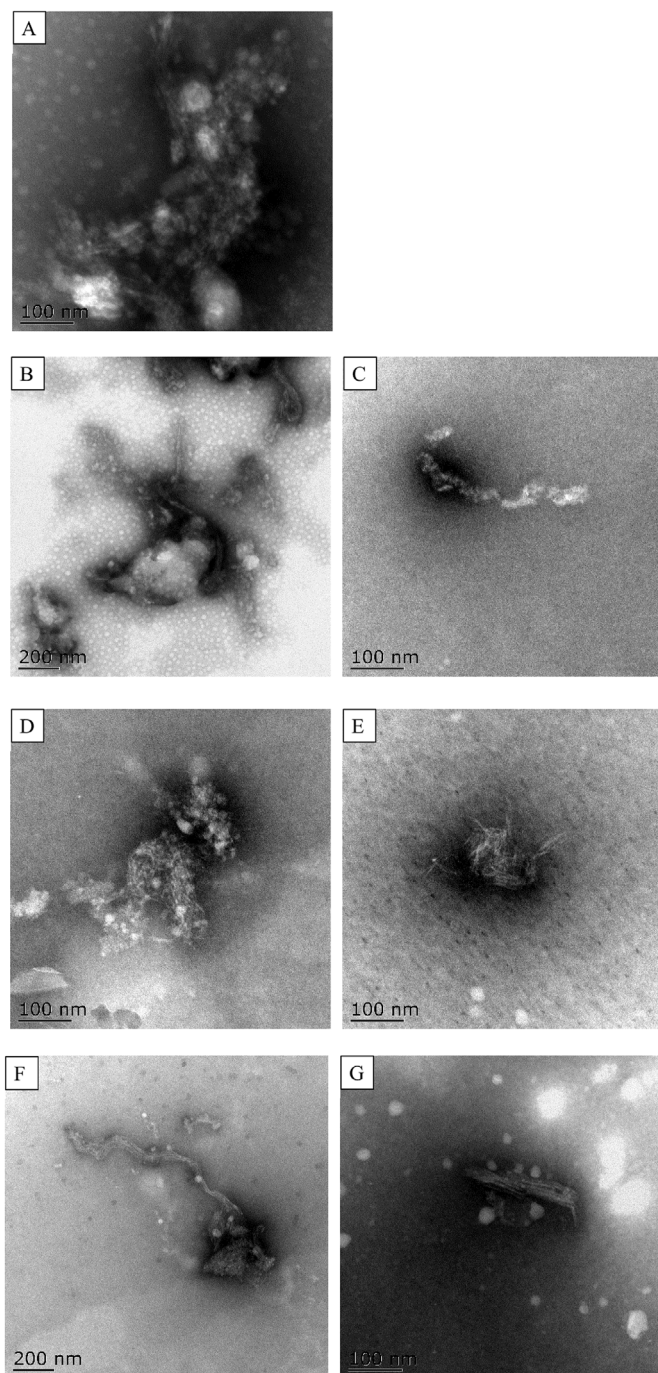


Fig. 6. Microstructures of myofibrillar protein (MP) suspensions treated at various high pressure homogenization (HPH) disruption chamber geometries. Note: A: Control (non-HPH treated sample); B: Z5 configuration (103 MPa); C: Z5 configuration (172 MPa); D: Z5-cf configuration (103 MPa); E: Z5-cf configuration (172 MPa); F: Z8-cf configuration (103 MPa); G: Z8-cf configuration (172 MPa).

Anton, 2004; Wang et al., 2017; Xue et al., 2017). HPH can cause the unfolding of myosin and expose hydrophobic residues, thus resulting in the loss of α -helix in MPs in water. In turn, the loss of the α -helix structure in the myosin rod region might cause a change in the interactions between the molecules, disrupting the filament assembly process, leading to enhanced solubility in water (Chen et al., 2016a). It can be assumed that the effect of disruption chamber geometries on MP secondary structure was different at various HPH pressures. The narrow bore diameter of the nozzle is more likely to destroy the secondary

Table 5
Surface hydrophobicity of myofibrillar protein (MPs) in water after 103 MPa and 172 MPa high pressure homogenization (HPH) treatment with different disruption chambers.

Pressure (MPa)	Surface reactive sulfhydryl contents ($\mu\text{mol}/100\text{ mg}$)		
	Z5	Z5-cf	Z8-cf
0	4.54 ± 0.63^g	4.54 ± 0.63^g	4.54 ± 0.63^g
103	11.20 ± 0.14^e	11.57 ± 0.37^d	9.85 ± 0.31^f
172	13.67 ± 0.24^a	12.29 ± 0.47^c	12.77 ± 0.21^b

Note: Values were mean of triplicate values \pm S.D. Different letter in row indicate statistical differences ($P < 0.05$).

Control: non-HPH treated sample; Z5: 130 μm nozzle and standard flow; Z5-cf: 130 μm nozzle and counter flow; Z8-cf: 200 μm nozzle and counter flow.

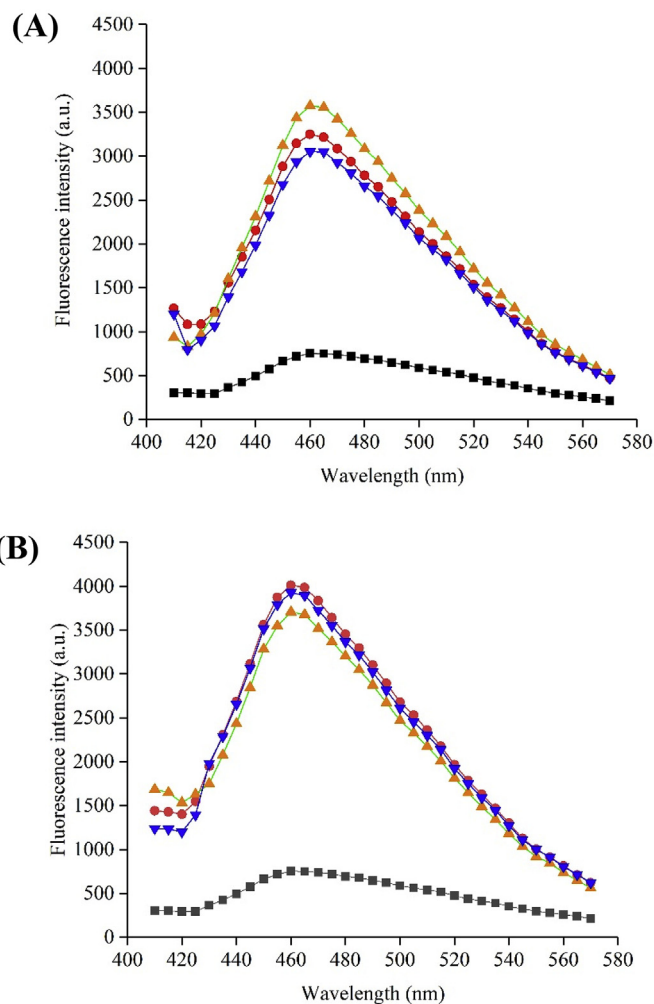


Fig. 7. Hydrophobicity of myofibrillar proteins (MPs) in water treated at 103 MPa (A) and 172 MPa (B) high pressure homogenization (HPH) treatment with different disruption chamber geometries. Note: Control (black square); Z5 configuration (red circle); Z5-cf configuration (orange triangle); Z8-cf configuration (blue triangle). (For interpretation of the references to colour in this figure legend, the reader is referred to the Web version of this article.)

structure of MPs under low pressure, whereas at higher pressure, the secondary structure is more damaged, and the bore diameter of the nozzle has no effect on the secondary structure.

4. Conclusion

As obtained from the current study, the nozzle and counter flow chamber have different effects on the solubility and protein structures

Table 6

Composition of secondary structures of myofibrillar protein (MPs) after 103 MPa and 172 MPa high pressure homogenization (HPH) treatment with different disruption chambers.

	Secondary structure (%)			
	α -helix	β -sheets	turn	Rndm. Coil
Control	58.4	10.8	13.1	17.7
Z5 (103 MPa)	45.5	12.6	15.4	26.5
Z5 (172 MPa)	42.4	13.8	16.5	27.3
Z5-cf (103 MPa)	44.9	12.8	15.5	26.8
Z5-cf (172 MPa)	41.4	14.1	15.9	28.6
Z8-cf (103 MPa)	50.5	11.2	14.2	24.1
Z8-cf (172 MPa)	42.0	13.8	15.7	28.3

Note: Control: non-HPH treated sample; Z5: 130 μ m nozzle and standard flow; Z5-cf: 130 μ m nozzle and counter flow; Z8-cf: 200 μ m nozzle and counter flow.

of MPs in water at different high hydrostatic pressures. The nozzles and counter flow chamber played a major role in the solubility of MPs in water at 103 MPa and 172 MPa HPH, respectively. Overall, the solubility of MPs in water could be improved more effectively by applying a narrow nozzle (Z5) when the HPH pressure was 103 MPa. As the pressure increased to 172 MPa, the counter flow chamber (Z5-cf, Z8-cf) could further damage the protein structure and reduce the particle size of MPs in water. The results showed that the solubility and stability of MPs in water can be regulated by designing the disruption chamber geometry, which provides a controllable strategy on meat protein processing. Our initial intention of applying HPH to MPs is to improve its solubility in water, which eliminate the impacts of high-salt intake on human health. However, the specific application of this technique to MPs need further study to maximize its benefits to the food industry.

Acknowledgments

We gratefully acknowledge the National Center of Meat Quality and Safety Control for providing research conditions. This work was financially supported by the National Natural Science Foundation of China (Grant No. 31671875) and a project funded by the Priority Academic Program Development of Jiangsu Higher Education Institutions (PAPD, No. 080–809001).

References

- Alvarez-Sabatel, S., Marañón, I. M. D., & Arboleya, J. C. (2015). Impact of high pressure homogenization (HPH) on inulin gelling properties, stability and development during storage. *Food Hydrocolloids*, *44*, 333–344.
- Chapleau, N. J., & de Lamballerie-Anton, M. (2003). Changes in myofibrillar proteins interactions and rheological properties induced by high-pressure processing. *European Food Research and Technology*, *216*(6), 470–476.
- Chapleau, N., Mangavel, C., Compoint, J. P., & de Lamballerie-Anton, M. (2004). Effect of high-pressure processing on myofibrillar protein structure. *Journal of the Science of Food and Agriculture*, *84*(1), 66–74.
- Chen, X., Chen, C. G., Zhou, Y. Z., Li, P. J., Ma, F., Nishiumi, T., et al. (2014). Effects of high pressure processing on the thermal gelling properties of chicken breast myosin containing κ -carrageenan. *Food Hydrocolloids*, *40*, 262–272.
- Chen, X., Xu, X. L., Han, M. Y., Zhou, G. H., Chen, C. G., & Li, P. J. (2016a). Conformational changes induced by high-pressure homogenization inhibit myosin filament formation in low ionic strength solutions. *Food Research International*, *85*, 1–9.
- Chen, X., Xu, X. L., & Zhou, G. H. (2016b). Potential of high pressure homogenization to solubilize chicken breast myofibrillar proteins in water. *Innovative Food Science & Emerging Technologies*, *33*, 170–179.
- Donsi, F., Annunziata, M., & Ferrari, G. (2013). Microbial inactivation by high pressure homogenization: Effect of the disruption valve geometry. *Journal of Food Engineering*,

- 115*(3), 362–370.
- Donsi, F., Sessa, M., & Ferrari, G. (2012). Effect of emulsifier type and disruption chamber geometry on the fabrication of food nanoemulsions by high pressure homogenization. *Industrial & Engineering Chemistry Research*, *51*(22), 7606–7618.
- Dumay, E., Chevalier-Lucia, D., Picart-Palmade, L., Benzaria, A., Gràcia-Julà, A., & Blayo, C. (2013). Technological aspects and potential applications of (ultra) high-pressure homogenisation. *Trends in Food Science & Technology*, *31*(1), 13–26.
- Floury, J., Bellettre, J., Legrand, J., & Desrumaux, A. (2004). Analysis of a new type of high pressure homogeniser. A study of the flow pattern. *Chemical Engineering Science*, *59*(4), 843–853.
- Hayakawa, T., Ito, T., Wakamatsu, J., Nishimura, T., & Hattori, A. (2009). Myosin is solubilized in a neutral and low ionic strength solution containing l-histidine. *Meat Science*, *82*(2), 151–154.
- Ito, Y., Tatsumi, R., Wakamatsu, J. I., Nishimura, T., & Hattori, A. (2015). The solubilization of myofibrillar proteins of vertebrate skeletal muscle in water. *Animal Science Journal*, *74*(5), 417–425.
- Krishnamurthy, G., Chang, H. S., Hultin, H. O., Feng, Y., Srinivasan, S., & Kelleher, S. D. (1996). Solubility of chicken breast muscle proteins in solutions of low ionic strength. *Journal of Agricultural and Food Chemistry*, *44*(2), 408–415.
- Liu, H. H., & Kuo, M. I. (2016). Ultra high pressure homogenization effect on the proteins in soy flour. *Food Hydrocolloids*, *52*, 741–748.
- Liu, R., Wang, N., Li, Q., & Zhang, M. (2015). Comparative studies on physicochemical properties of raw and hydrolyzed oat β -glucan and their application in low-fat meatballs. *Food Hydrocolloids*, *51*, 424–431.
- Liu, W., Zhang, Z. Q., Liu, C. M., Xie, M. Y., Tu, Z. C., Liu, J. H., et al. (2010). The effect of dynamic high-pressure microfluidization on the activity, stability and conformation of trypsin. *Food Chemistry*, *123*(3), 616–621.
- Marco-Molés, R., Hernando, I., Llorca, E., & Pérez-Munuera, I. (2012). Influence of high pressure homogenization (HPH) on the structural stability of an egg/dairy emulsion. *Journal of Food Engineering*, *109*(4), 652–658.
- Nieuwenhuizen, W. F., Weenen, H., Rigby, P., & Hetherington, M. M. (2010). Older adults and patients in need of nutritional support: Review of current treatment options and factors influencing nutritional intake. *Clinical Nutrition*, *29*(2), 160–169.
- Ronkart, S. N., Paquot, M., Deroanne, C., Fougny, C., Besbes, S., & Blecker, C. S. (2010). Development of gelling properties of inulin by microfluidization. *Food Hydrocolloids*, *24*(4), 318–324.
- Saricaoglu, F. T., Gul, O., Tural, S., & Turhan, S. (2017). Potential application of high pressure homogenization (HPH) for improving functional and rheological properties of mechanically deboned chicken meat (MDCM) proteins. *Journal of Food Engineering*, *215*, 161–171.
- Sharp, A., & Offer, G. (1992). The mechanism of formation of gels from myosin molecules. *Journal of the Science of Food and Agriculture*, *58*, 63–73.
- Song, X. Z., Zhou, C. J., Wu, Q. L., Fu, F., & Chen, Z. L. (2013). Effect of high-pressure homogenization on particle size and film properties of soy protein isolate. *Industrial Crops and Products*, *43*(1), 538–544.
- Sørensen, H., Mortensen, K., Sørland, G. H., Larsen, F. H., Paulsson, M., & Ipsen, R. (2014). Dynamic ultra-high pressure homogenisation of milk casein concentrates: Influence of casein content. *Innovative Food Science & Emerging Technologies*, *26*, 143–152.
- Takai, E., Yoshizawa, S., Ejima, D., Arakawa, T., & Shiraki, K. (2013). Synergistic solubilization of porcine myosin in physiological salt solution by arginine. *International Journal of Biological Macromolecules*, *62*, 647–651.
- Tokifuji, A., Matsushima, Y., Hachisuka, K., & Yoshioka, K. (2013). Texture, sensory and swallowing characteristics of high-pressure-heat-treated pork meat gel as a dysphagia diet. *Meat Science*, *93*(4), 843–848.
- Wang, M. Y., Chen, X., Zou, Y. F., Chen, H. Q., Xue, S. W., Qian, C., et al. ... Zhou, G. H. (2017). High-pressure processing-induced conformational changes during heating affect water holding capacity of myosin gel. *International Journal of Food Science and Technology*, *52*(3), 724–732.
- Xue, S. W., Yang, H., Wang, H. H., Tendu, A. A., Bai, Y., Xu, X. L., et al. ... Zhou, G. H. (2017). High-pressure effects on the molecular aggregation and physicochemical properties of myosin in relation to heat gelation. *Food Research International*, *99*, 413–418.
- Zamora, A., & Guamis, B. (2015). Opportunities for ultra-high-pressure homogenisation (UHPH) for the food industry. *Food Engineering Reviews*, *7*(2), 130–142.
- Zhang, Z. Y., Yang, Y. L., Tang, X. Z., Chen, Y. J., & You, Y. (2015). Chemical forces and water holding capacity study of heat-induced myofibrillar protein gel as affected by high pressure. *Food Chemistry*, *188*, 111–118.
- Zhao, Y. Y., Wang, P., Zou, Y. F., Li, K., Kang, Z. L., Xu, X. L., et al. (2014). Effect of pre-emulsification of plant lipid treated by pulsed ultrasound on the functional properties of chicken breast myofibrillar protein composite gel. *Food Research International*, *58*(4), 98–104.
- Zhong, J., Liu, X. W., Wei, D. X., Yan, J., Wang, P., Sun, G., et al. (2015). Effect of incubation temperature on the self-assembly of regenerated silk fibroin: A study using AFM. *International Journal of Biological Macromolecules*, *76*, 195–202.